inventions

MDPI

Article

An Original Aerodynamic Ducting System to Improve Energy Efficiency in the Automotive Industry

Jana Fernández-Gutiérrez, Pablo Fernández-Arias, Diego Vergara * and Álvaro Antón-Sancho

Technology, Instruction and Design in Engineering and Education Research Group, Catholic University of Ávila, C/Canteros s/n, 05005 Ávila, Spain

* Correspondence: diego.vergara@ucavila.es

Abstract: In the automotive industry, the flow of air generates high resistance in the advance of vehicles. In light of this situation, the objective of the present invention is to take advantage of the force of the air itself to help propel vehicles and thus reduce fuel consumption. A channeling system has been designed based on a deflector that collects the air that impacts against the vehicle at the front, transferring it to the rear where it is expelled, allowing the vacuum zone to be filled so that the high pressures of the channeled air are repositioned in the depression zone, significantly increasing the values of the pressures, including those that were previously negative. The deflector has been built and incorporated into a model car so that comparative experimental wind tunnel tests could be carried out to verify that the vacuum in the rear area is eliminated, and positive pressure is obtained.

Keywords: automotive; wind tunnel; air ducting; energy efficiency

Citation: Fernández-Gutiérrez, J.; Fernández-Arias, P.; Vergara, D.; Antón-Sancho, Á. An Original Aerodynamic Ducting System to Improve Energy Efficiency in the Automotive Industry. *Inventions* **2023**, *8*, 13. https://doi.org/10.3390/inventions8010013

Academic Editor: Shyy Woei Chang

Received: 30 November 2022
Revised: 29 December 2022
Accepted: 3 January 2023
Published: 6 January 2023

1. Introduction

By 2030, the global car fleet will grow from 800 million to 1.6 billion vehicles [1]. This doubling of the global car fleet requires a radical technological change to ensure long-term sustainable mobility in line with the goal of eliminating carbon emissions from transport. The strategy should therefore help European industry to lead the global development of alternative propulsion technologies. Given that the mobility sector is responsible for a large part of the EU's total greenhouse gas emissions, the Green Deal [2], the European Union (EU) mechanism for the transformation of the energy system [3], and the development of a green and sustainable economy in a post-COVID-19 scenario [4] has, as its main objectives, to reduce greenhouse gas (GHG) emissions by at least 55% by 2030 and to reduce greenhouse gas (GHG) emissions by 90% by 2050, achieving climate neutrality [2] to strengthen sustainable development [5].

To this complex scenario must be added the fact that, as global emissions are becoming more and more worrying, the regulations for greenhouse gases and air quality imposed on vehicles to comply with emissions targets according to the European vehicle type approval procedure WLTP (World Harmonized Light-duty Vehicle Test Procedure) [6] are correspondingly stricter [7].

Therefore, it is necessary to propose strategies to improve the efficiency of current vehicle designs, and one of the areas of work is in the improvement of the aerodynamic efficiency of moving vehicles, which also benefits all types of current passenger vehicles regardless of the type of propulsion they use. One of the main problems with the aerodynamics of today's vehicles is airflow, as the impact of air on moving vehicles causes high resistance to movement. One solution to optimize vehicle efficiency and reduce energy consumption is to reduce aerodynamic drag, which has been studied from the point of view of numerical optimization [7], technical design [8], the development of specific algorithms [9], and which has a quadratic relationship with the driving speed [10].

Several studies have concluded that proper vehicle design would be necessary to decrease the aerodynamic drag generated at the rear of vehicles [11]. In this sense, the

literature identifies works focused on different vehicle devices, such as the state of the wheels [12] or the use of flaps [13]. Since air is a great source of energy in other energy systems such as wind energy, the concern of this research stems from the objective of taking advantage of the great force of the airflow impinging on vehicles, to transform a part of the problem into a competitive advantage. In addition, the study also arises from the concern of needing to reduce the use of various types of fuels, due to the great environmental and socioeconomic problems that they entail both in the present and in the future.

To reduce aerodynamic drag, several studies have analyzed the structural modification of vehicles [14], for example, by studying the influence of the wheels [15], the influence of flaps [16], or performing different types of rounding in the outer parts of the rear area, some of the purposes being the control of vortices [17], turbulence [18], boundary layer or drag force [19].

Likewise, there are lines of research [10] that seek to reduce aerodynamic drag by developing different deflector models, each of which is validated with CFD computational simulation, which allows a better understanding of the behavior of the air in different situations. These studies develop passive [20] or active methods [21] to reduce aerodynamic drag or analyze the influence of certain moving vehicle components on aerodynamic drag [22]. Therefore, with the common aim of reducing aerodynamic drag, the present paper focuses on the pressure difference between the front and rear of a car, which is the main cause of aerodynamic drag [23], intending to decrease this difference by increasing the air pressure at the rear. Several studies [24] have developed this idea by "base bleed", inserting air channeling ducts that longitudinally cross the entire vehicle located inside the vehicle in the base region, and have used this idea to achieve fuel efficiency increases [25] or to reduce aerodynamic drag [26]. However, the present research analyzes the incorporation of a ducting system based on a deflector that is placed on top of vehicles, without requiring internal structural changes to the vehicle.

As can be noticed in Figure 1a, the air trajectory at the rear of vehicles approximately follow the red arrows, so that a vacuum is generated, that is, a suction between the vehicle and the air trajectory, which acts as a brake on forward motion. Therefore, after identifying the problem, the objective developed in the present investigation is based on the deflector located at the top of the vehicle, capturing and channeling the incident air at the front and redirecting it to the rear, to fill the suction area with positive pressure, as indicated by the green arrows in Figure 1b.

(**a**) (**b**)

Figure 1. Air flow path: (**a**) vehicle without deflector; (**b**) vehicle with built-in deflector.

The act of channeling air from the upper part has already been verified computationally [27], however, it was based on making a groove on the roof of the vehicle itself, unlike the present research, which is based on anchoring a deflector to the roof of the vehicle that allows a greater volume of incident air to be captured and channeled. In addition, the present study has been experimentally verified, promoted mainly because there is insufficient theoretical information available for the equations that govern fluid mechanics in certain new circumstances with interest in investigating new behaviors; this forces automotive aerodynamics to be a predominantly experimental science since, in this way, real-world values are measured and assessed, which provides a lot of additional value to computational simulations, which are a valuable tool in themselves. Because of this, several studies analyze aerodynamic variables such as drag coefficient [28], vortices [29], turbulence [30], boundary layer, or stability [31], through experimental testing. The preced-

ing literature also proved that prototypes such as the one presented here are also interesting in the evaluation of fatigue life [32,33], and lateral stability improvement [34].

2. Materials and Methods

With the objective of designing a deflector capable of taking advantage of the great force of airflow that hits the front of a moving vehicle and transferring it to the rear of the vehicle, thus reducing fuel consumption, the present research has been structured in the following phases (Figure 2): (i) Phase I: design of the deflector; (ii) Phase II: aerodynamic simulations; (iii) Phase III: mechanical design and construction; and (iv) Phase IV: experimental tests. The methodology illustrated in Figure 2 is based on previous papers which followed similar methodologies for studying other inventions [35].

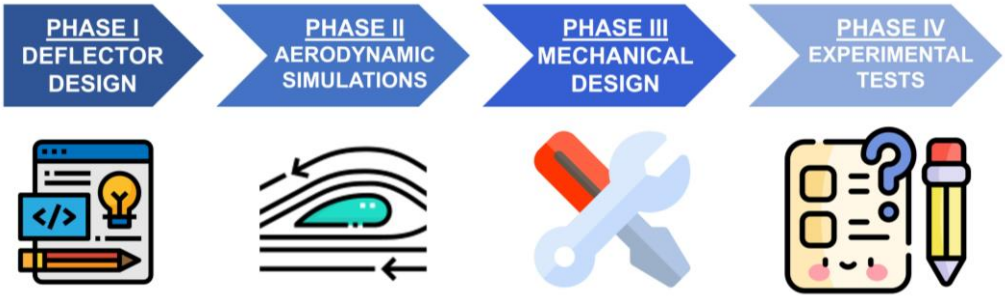

Figure 2. Research methodology outline.

In the design phase of the deflector in 3D software (Phase I, Figure 2), the upper deflector was designed in Autocad 3D®. Likewise, a vehicle considered a model (Figure 3a) was designed in the same software, and the deflector system was incorporated in parallel to this model (Figure 3b).

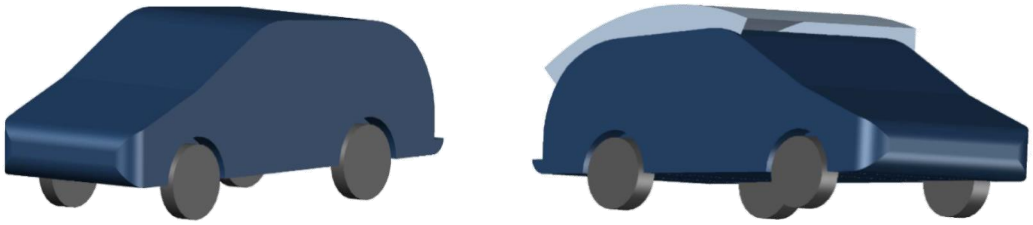

(**a**) (**b**)

Figure 3. Autocad 3D® design: (**a**) vehicle without deflector; (**b**) vehicle with incorporated deflector.

In the aerodynamic simulations phase (Phase II, Figure 2), Autodesk Flow Design® was used to perform different aerodynamic simulations, subjecting the vehicle without the deflector to the same aerodynamic conditions previously defined, and then the vehicle with the deflector designed in Phase I, to analyze the difference in the behavior of the airflow for both the conventional vehicle and vehicle with the deflector system incorporated.

To then experimentally validate the results obtained in the computational simulation [36], the deflector was mechanically designed and built (Phase III, Figure 2) to fit a 1:12 scale model car, which was also specifically designed and built (Figure 4). In the figure images, the model car appears with the deflector system already incorporated; however, it can be easily removed and put on due to a groove made on each upper side. The wheels used were made with ball bearings to ensure adequate mobility. The channeling system design was based on a deflector with a curvature that allows the internally circulating airflow to maintain, as much as possible, uniformity of projection to avoid turbulence. This design allowed air to be captured from the front, from the hood, and in turn, from the roof, with the three edges of the deflector having a water drop profile [37,38] in section and front curvature to favor aerodynamics. In turn, the rear shape of the deflector has a downward curvature, which forces the projection of airflow circulating inside the deflector

to descend to the vacuum area when it leaves the duct because its geometry forces the redirection of air to the rear area of the car near the wall of the same. In addition, an open suction wind tunnel with a closed test chamber (Figure 5), with a useful working section of 35 cm × 40 cm × 100 cm, was designed and built.

(**a**) (**b**)

Figure 4. Car model with built-in deflector: (**a**) front side; (**b**) rear side.

Figure 5. Wind tunnel design.

Finally, in Phase IV, the experimental testing phase (Figure 2), the model with and without the deflector was subjected to different airflow conditions in various experimental tests. The objective was to measure the pressure at the rear of the vehicle model since this area is the most affected by the deflector duct system, and it is of interest to analyze the values of the pressure variations in this area. The measurements were made using a water column, therefore, the upper lid of the test chamber was made of wood instead of methacrylate to allow the Pitot tube to be introduced through the various holes drilled in the wood (Figure 6), which allowed measurements to always be taken in the same places.

The selected measurement points were established in the same plane at different points at the rear area of the vehicle with the same common distance from the end of the vehicle; a total of nine different points were determined that sufficiently allowed the behavior of the air on the model with and without the deflector to be defined, measured, analyzed, and compared.

Figure 7a shows the plane on which the nine points were measured. The test points were referenced to an XYZ coordinate system so that the X-axis represented the separation distance from the end of the vehicle, the Y-axis the height measured from the ground, and the Z-axis the transverse distance whose origin is located at the lateral edge of the model (cf. Figure 7a).

It should be noted that the notation used in this study is X*i*, Y*j*, and Z*j*, where X, Y, and Z are the previously defined Cartesian axes, *i* denotes the distance in cm from the origin on the X-axis, and *j* denotes the distance in mm from to the origin in the Y and Z axes. Thus, from Figure 7a, the coordinates of the different points can be established in the following

points (Table 1): three points defined on the Z-axis at 20 mm, 60 mm, and 100 mm from the coordinate origin (Z20, Z60, and Z100, respectively), and another three points on the Y-axis, at 35, 65, and 95 mm from the origin (Y35, Y65, and Y95, respectively). This constitutes a measurement plane formed by a 3 × 3 matrix with nine points (A, B, C, D, E, F, G, H, and I) according to Table 1.

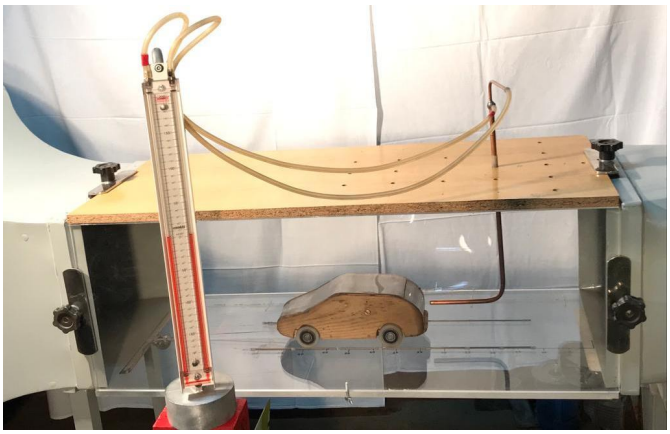

Figure 6. Measuring system.

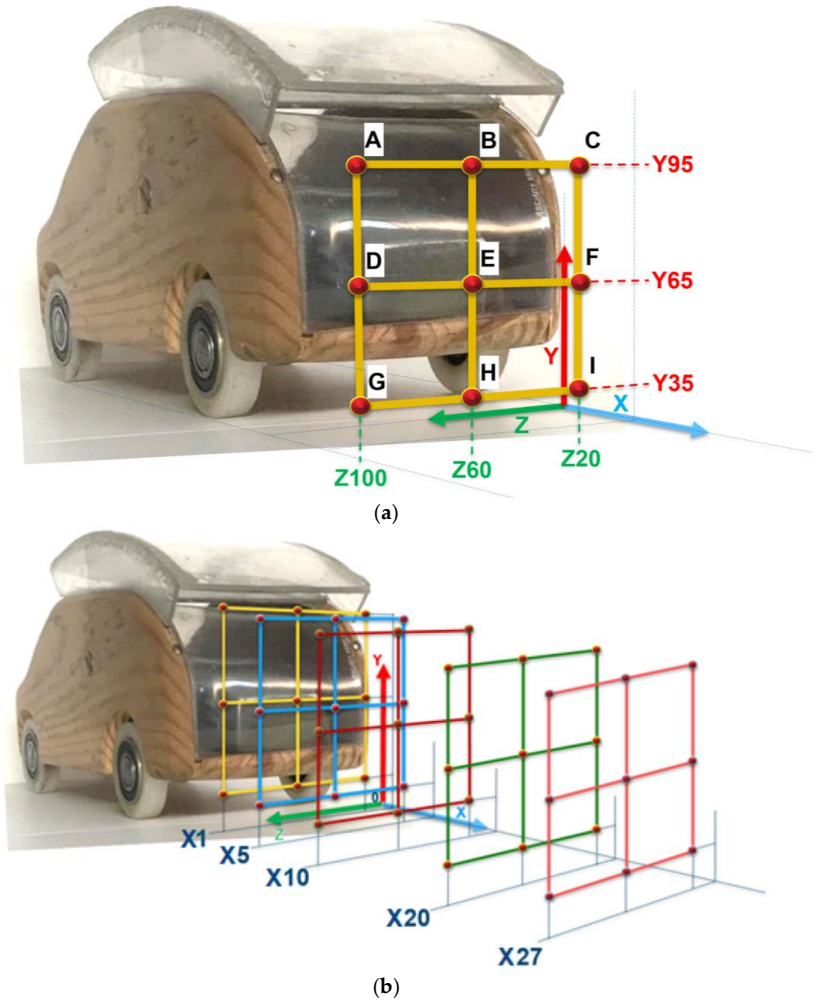

Figure 7. Measuring points: (**a**) on the YZ plane; (**b**) on the air wake (X-axis).

Table 1. Measurement points in the various planes.

	Z100	Z60	Z20
Y95	A	B	C
Y65	D	E	F
Y35	G	H	I

In addition, it was deemed necessary to take measurements at different distances from the rear end of the model (X-axis), in order to improve the determination of the airflow wake and thus be able to analyze the influence of incorporating the aerodynamic ducting system. The distances thus considered in the X-axis were 1 cm, 5 cm, 10 cm, 20 cm, and 27 cm, resulting in planes X1, X5, X10, X20, and X27, respectively (Figure 7b). As each of these five distances establish the nine measurement points that make up each measurement plane (Table 1), a total of 45 measurement points were considered in this study.

As a last step, all measurements were repeated at three different air speeds supplied by the wind tunnel at a laminar flow in the test chamber, so that the influence of airflow speed on the efficiency of the ducting system could be analyzed. The first speed was equivalent to a vehicle speed of 35 km/h (equivalent to 6 mm H_2O), the second speed equivalent to 41 km/h (equivalent to 8 mm H_2O), and the third speed equivalent to 50 km/h (equivalent to 12 mm H_2O).

The criterion to establish the three airflow speed values was based primarily on the fact that the maximum speed that the wind tunnel could supply using the 2 kW suction fan, and guaranteeing at all times that the airflow had the optimum laminar flow conditions in the testing chamber, was 50 km/h. Therefore, the value of 50 km/h was set as necessary to evaluate the model at the maximum achievable speed. In addition, a minimum speed value of 35 km/h was set based on previous measurements in which the authors observed that below 35 km/h, the pressure values obtained were less relevant. Finally, to enhance the analysis of air behavior in the wake of the model, it was considered appropriate to measure at a third speed of 41 km/h between the maximum and minimum speed values.

Thus, the selection of 45 points and 3 different speeds yielded 135 measurement cases. Additionally, two pressure measurements were taken at each of the 135 measurement cases, one with and one without the deflector. Therefore, a total of 270 different pressure values were analyzed in this research work.

3. Results and Discussion

First, the results of the computational simulations carried out using Autodesk Flow Design® software are shown. In Figure 8a, the mock-up of the conventional vehicle is shown, where the wake left by the vehicle as it moves forward is dark blue. However, in Figure 8b, the mock-up has the deflector system incorporated in the upper part and it can be seen that the deflector manages to provide a different wake to the rear of the vehicle, represented by the additional light blue area.

Likewise, Figure 9 shows in greater detail the direction of the airflow lines in the simulation of the vehicle in motion incorporating the deflector, showing that at the exit of the deflector, the air is redirected toward the lower rear part of the model.

The data were obtained from the average of 270 measurements (Appendix A), structured mainly in seven blocks: (i) point in the plane at which the values are taken (Figure 7a); (ii) measurement distance from the end of the vehicle (distance on the X-axis); (iii) speed supplied by the wind tunnel to the mock-up located in the test chamber, (V); (iv) measurement height from the ground (distance on the Y-axis); (v) 135 pressure values measured with the conventional mock-up without deflector at each measurement point—this block is subdivided into three columns because each of them represents the distance from the origin of the Z-axis (Figure 7a); (vi) 135 pressure values with the incorporation of the deflector system to the model—this block is also subdivided in three columns due to the fact that each of them show the distance from the origin of the Z-axis (Figure 7a); and (vii) comparison of

pressure without deflector (P_α) and with deflector (P_β) at each of the nine points measured, indicating the respective pressure difference ($P_\beta - P_\alpha$) at each measurement point. In turn, this last block was subdivided into three columns because each of them indicated the distance from the origin of the Z-axis (Figure 7a).

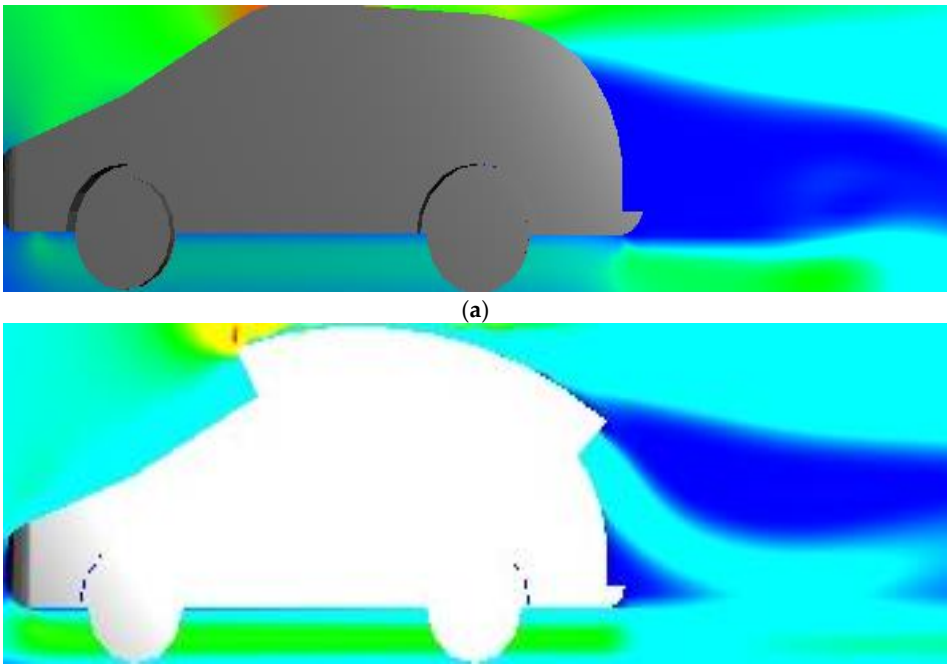

(**a**)

(**b**)

Figure 8. Vehicle wake: (**a**) without deflector; (**b**) with deflector.

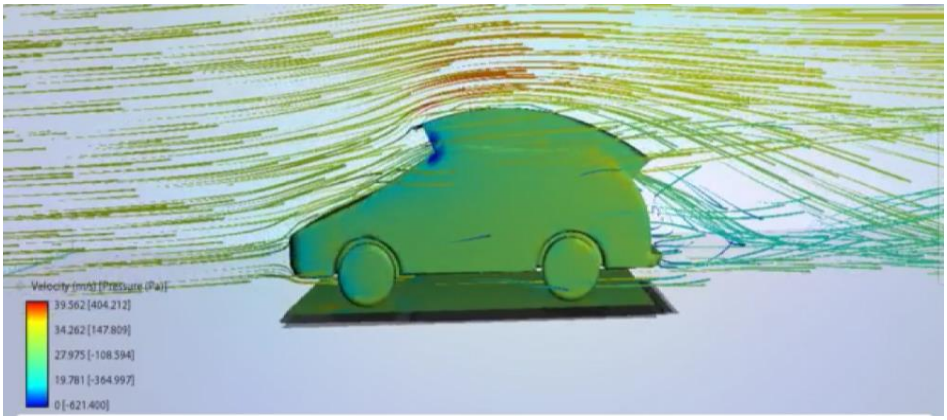

Figure 9. Direction of airflow lines with deflector.

First, using the computational simulation with the Autodesk Flow Design® software, as shown in Figure 8, it can be seen that the upper deflector captured and channeled the airflow that hit the front of the vehicle, and in taking advantage of its force and transferring it to the rear area, a new airflow appears in the wake left by the vehicle, with positive pressures that manage to fill a previously empty area that consisted of only negative pressures. This concept corresponds to that obtained in the studies [24,25], which implemented a similar channeling system, also taking advantage of the incident air at the front of the vehicle; nevertheless, the arrangement of the ducts is different since they are located inside the bottom of the vehicle. However, this study [27] did also have a duct at the top based on a slot in the roof, which verifies the effect.

Second, the results obtained from the experimental tests were analyzed, observing mainly that in the measurements taken from the conventional model without deflector, 40%

of the pressures have negative values; however, in the results of the measurements from the model incorporating the upper deflector system, 100% of the pressures have positive values, thus achieving the fundamental objective of this study. This had been achieved because it was possible to significantly increase the value of the pressure at the rear area of the vehicle, thereby eliminating all the negative pressures that generated the vacuum zone.

Next, the analysis of the airflow behavior was deepened using the results obtained from the experimental tests. Appreciating the difference in pressures ($P_\beta - P_\alpha$, Appendix A) at the 135 measured points, and considering the subtraction of the deflector pressure values from those measured without, it was revealed that all values were positive or at least 0, which indicates that 60% of the initial positive values without the deflector had a lower magnitude than the values with deflector. Therefore, at all of these measuring points, the deflector also provides a great advantage, since it favors vehicle thrust. This fact also then implies that at all of the measured points, the deflector redirects an airflow that allows the pressure in the entire analyzed wake to increase, effectively managing to propel the car.

The values computed as the difference in pressures ($P_\beta - P_\alpha$, Appendix A), besides being all positive at each point compared, in many cases reached values of high magnitude, even significantly exceeding the magnitude of the absolute value of the pressures obtained without the deflector. Likewise, the pressures found from the pressure difference (calculated as $P_\beta - P_\alpha$) represent the pressure with which the vehicle can be propelled forward at that point, which is equivalent to having an airflow of, for example, 7 mm H_2O or its equivalent vehicle speed of 38 km/h, propelling the vehicle from the rear in its direction of travel. The maximum pressure difference ($P_\beta - P_\alpha$) value obtained was 15 mm H_2O (at a speed of 50 km/h, in the plane located 1 cm from the X-axis (X1), at a height of 95 mm from the Y-axis (Y95) at 60 mm from the Z-axis (Z60)), which translates to driving the vehicle with an airflow of 55 km/h.

When comparing the pressure measurements with the speed (Figure 10) and with respect to the X-axis (Figure 7), i.e., the distance from the model at which it has been measured, the evolution of the pressure values with and without the deflector can be observed. In turn, to know the pressure evolution with speed, the pressures were analyzed at each of the three speeds (V): at 35 km/h (Figure 10a), at 41 km/h (Figure 10b), and at 50 km/h (Figure 10c). The mean pressure values of each of the five planes (X1, X5, X10, X20, and X27) were represented as ordinates, each plane being made up of nine pressure measurements.

Firstly, it was observed that the three series of pressure measurements without the deflector started with negative pressure values, and as the measurement point moved away from the vehicle, positive pressure values increased. At the same time, the pressure series with the deflector also tended to increase, although it can be seen that at the start, they were already positive values and it ended with positive values of greater magnitude compared to those measured without the deflector. The geometry of the three graphs of the series with and without the deflector are relatively similar. As a result, the higher the speed, the greater the distance between the corresponding series. The comparative gain achieved by the deflector in terms of speed is equivalent to the surface area between the series with deflector and the series without deflector in each of the three graphs in Figure 10. Therefore, it was determined that, at higher speeds, larger pressure differences are achieved thanks to the flow captured, channeled, and redirected by the deflector, which implies that the efficiency of the deflector system increases as the vehicle speed increases.

In the area of the wake closest to the end of the model (measurements made in the planes located at X1, X5, and X10 according to Figure 10), the greatest gain was observed as higher pressures were obtained, which implies a greater decrease in aerodynamic drag. At the same time, it was observed how the pressures progressively attenuated as the measurement point moves further away from the end of the vehicle. Therefore, the advantage of the recirculating air from the deflector exists until at least a distance of 27 cm from the rear of the vehicle, which is the last distance that has been considered significant. In turn, the magnitude of the deflector recirculated airflow effect decreases as

the measurement separation distance increases, which is consistent with the computational simulation reflected in Figure 8.

On the other hand, the pressure values obtained with respect to the Y-axis of the measurement reference points (Figure 7) are examined, so that according to Figure 11, the three series of measurements associated with the three coordinates without the deflector following similar trajectories in the three graphs at 35 km/h (Figure 11a), 41 km/h (Figure 11b), and 50 km/h (Figure 11c). However, when considering the deflector, the Y95 coordinate is significantly higher than the other two lower coordinates Y65 and Y35, which implies that the highest pressure contributions provided by the deflector-channeled air are achieved at a height of Y95 mm. This effect is because this is the zone where the airflow channeled by the deflector arrives with higher velocity and pressure so that in the lower coordinates of Y65 and Y35, it is perceived that the airflow is losing potential as it dissipates.

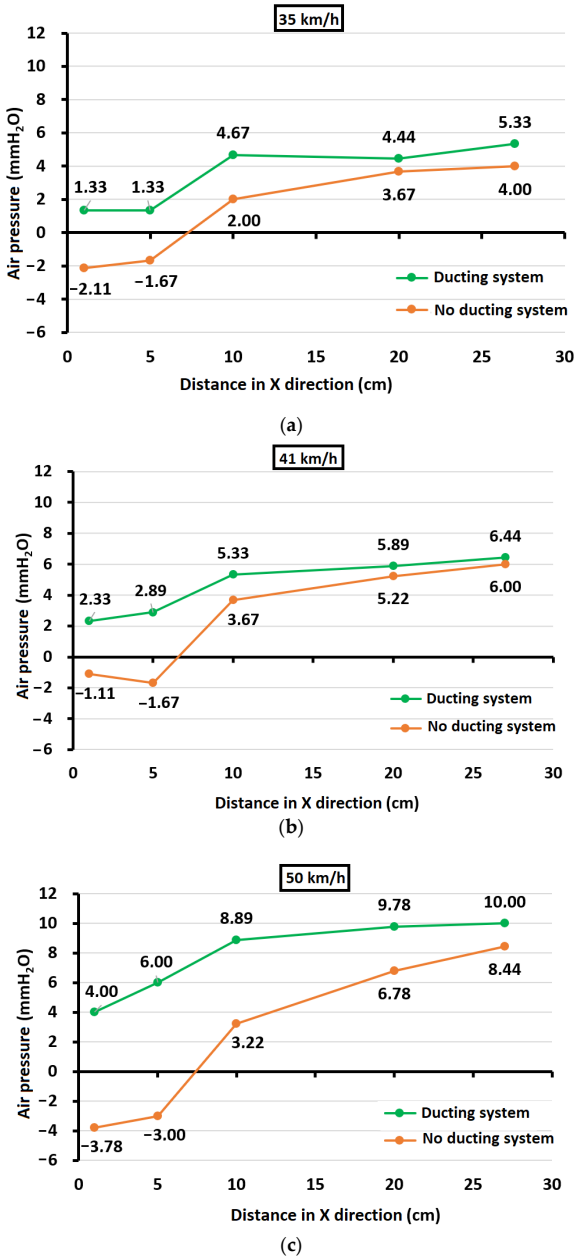

Figure 10. Comparison of pressures with and without deflector with respect to the X-axis at different velocities (V): (**a**) 35 km/h; (**b**) 41 km/h; and (**c**) 50 km/h.

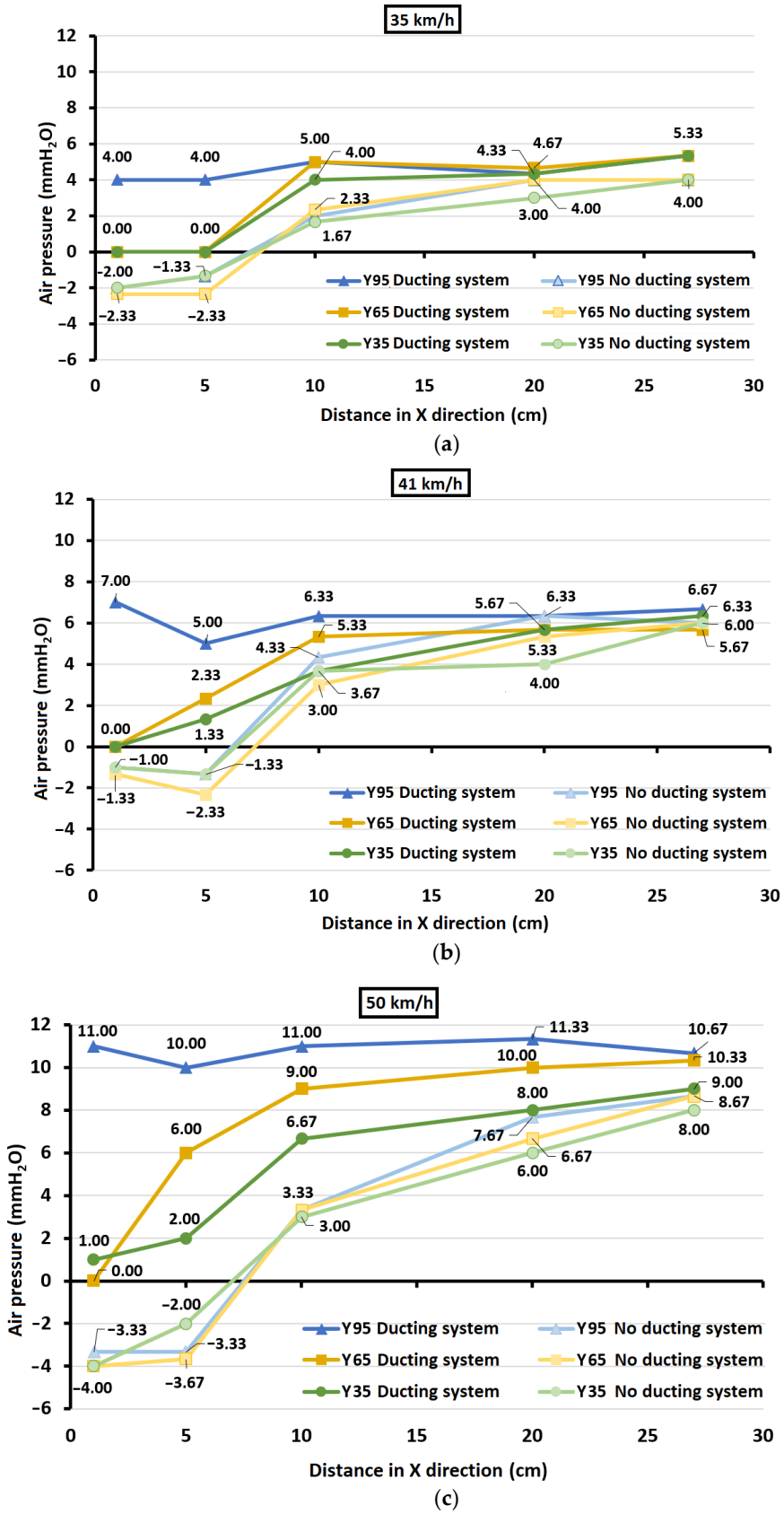

Figure 11. Comparison of pressures with and without deflector with respect to the Y-axis at different velocities (V): (**a**) 35 km/h; (**b**) 41 km/h; and (**c**) 50 km/h.

When analyzing the values of the pressures with respect to the Z-axis according to the established measurement points (Figure 7), it is observed in Figure 12 that the pressures in absolute values are higher in the central Z60 coordinate, both with and without deflector.

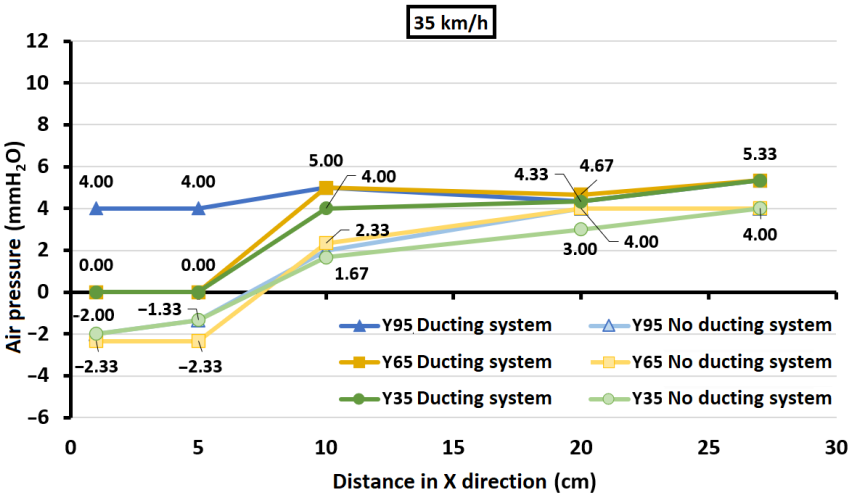

(**a**)

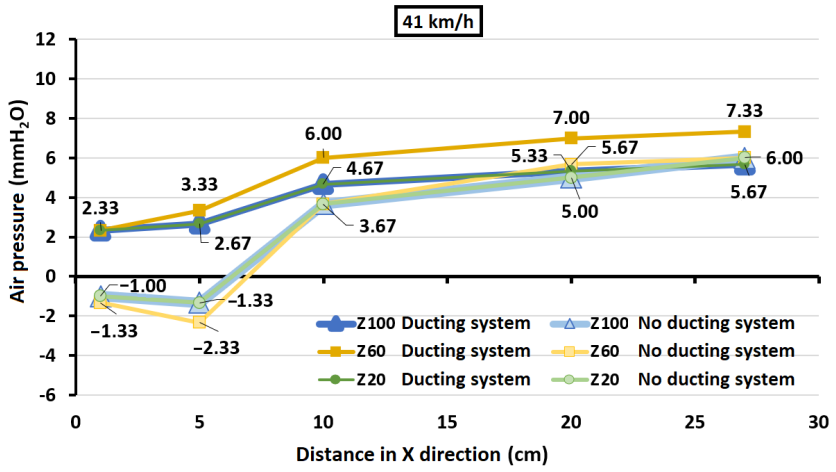

(**b**)

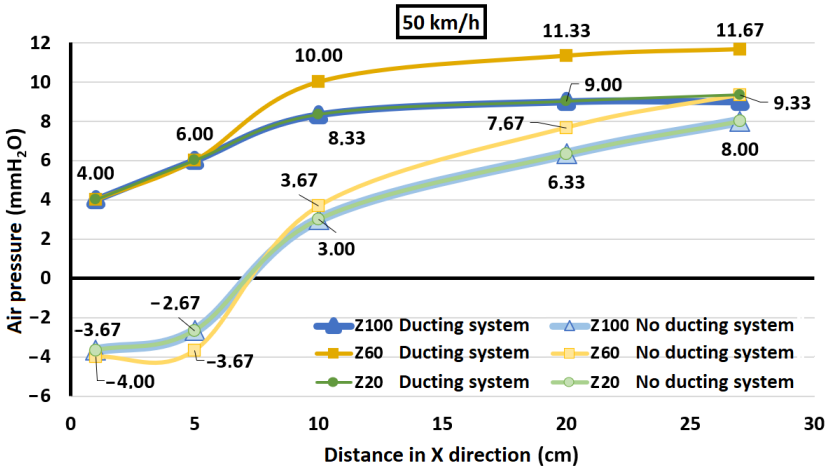

(**c**)

Figure 12. Comparison of pressures with and without deflector with respect to the Z-axis at different velocities (*V*): (**a**) 35 km/h; (**b**) 41 km/h; and (**c**) 50 km/h.

In addition, symmetry is manifested, the Z60 coordinate being the axis of symmetry, since the series associated with Z20 and Z100 overlap, which happens in both with and without deflector analyses, thus maintaining this effect despite the variation in speed represented in each of the three graphs of (a) 35 km/h, (b) 41 km/h, and (c) 50 km/h. This result was because the air from the sides contributes to bringing greater pressure to the central area, and in turn, for the coordinates Z20 and Z100, the full force of the air is not used because it is dispersed as it was closer to the end of the volume occupied by the vehicle.

An estimated measurement of the performance of this device could be made from the energy balance of the vehicle with and without the deflector. The forces involved in the vehicle motion are (i) rolling resistance (F_R), (ii) aerodynamic drag (F_A), (iii) slope resistance (F_S) (in this case a flat surface will be considered so $F_S = 0$), and (iv) thrust force (F_P).

Rolling resistance can be calculated from Equation (1):

$$F_R = k \cdot m \cdot g \tag{1}$$

where k is the dynamic friction coefficient, m is the vehicle mass, and g denotes gravity. It has been assumed that $k = 0.03$, which is the average value for a road in good condition [39], the mass m of the model is 0.99 kg, and that of the deflector is 0.12 kg.

The aerodynamic drag can be computed with Equation (2):

$$F_A = \frac{1}{2} \cdot C_x \cdot S \cdot r \cdot v^2 \tag{2}$$

where C_x represents the aerodynamic drag coefficient, assumed to be $C_x = 0.32$, considering the value given by manufacturers for a similar body model and that for most cars, $0.30 < C_x < 0.35$; S is the front surface of the vehicle affected ($S_\alpha = 0.\ 01426\ m^2$ in the case without deflector, and $S_\beta = 0.01612\ m^2$ for the case with deflector); r is the air density ($r = 1.225\ kg/m^3$, according to ISA (International Standard Atmosphere) at sea level and 15 °C); and v is the vehicle speed ($v = 50$ km/h = 13.89 m/s).

Equation (2) can also be used to obtain the value of F_P, but considering the thrust surface as half of the rear surface of the vehicle ($S = 0.00806\ m^2$), then the value of the velocity (v) at the rear area of the vehicle is obtained from the equation:

$$P = \frac{1}{2} \cdot r \cdot v^2 \tag{3}$$

where the average pressure P at the rear of the vehicle, for a speed of 50 km/h, can be obtained from Figure 13 and the following computations:

$$P_\alpha\ (X) = \frac{\int_0^{27} \left(-0.0144x^2 + 0.9032x - 5.4448\right) dX}{27} \tag{4}$$

$$P_\beta\ (X) = \frac{\int_0^{27} (0.0005x3 - 0.0339x2 + 0.8413x + 3.0273) dX}{27} \tag{5}$$

This way, the deflector's efficiency (η) could be considered about 3.8%, according to

$$\eta = \left(\frac{\left| F_\beta - F_\alpha \right|}{F_\alpha} \right) \cdot 100 = \frac{(\Delta F_A + \Delta F_R + \Delta F_P)}{(F_A + F_R)_\alpha} = 3.8\% \tag{6}$$

As a future study, it is proposed to carry out more experimental tests to define the wake that originated at the rear of the vehicle in greater detail, for example, by measuring in more planes and at different speeds. The wind tunnel will be optimized by adding a booster fan at the inlet to increase the speed in the test chamber. In turn, with this greater definition of the created effect, the calculation of the performance provided by this deflector system will be studied, analyzing all of the forces that influence the movement of the vehicle, so that the

energy balances of the conventional vehicle and vehicle with the deflector can be compared quantitatively. However, although at this moment the performance of the deflector system has not been quantified, its incorporation already indicates that the deflector will provide an economic saving, since the data already obtained verified that the pressures values were substantially improved, eliminating the resistance to the advance of the vehicle, thus directly implying a fuel saving.

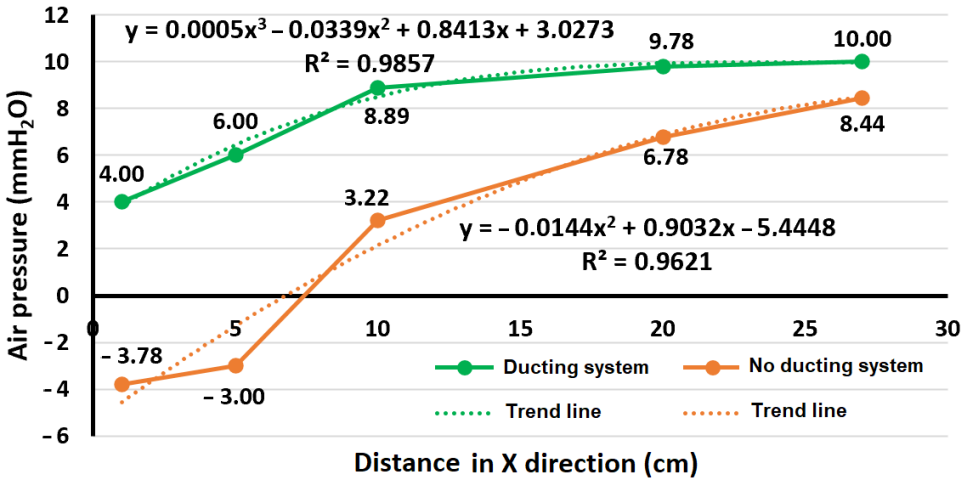

Figure 13. Adjustment of trend lines for pressures at 50 km/h.

The main difference between the prototype described and the actual product is the material since in the deflector model built for the experimental tests, methacrylate has been used, while in the real world, deflectors mass-produced in automotive companies from this prototype would be manufactured in fiberglass. However, both are quite similar materials and no alterations in airflow behavior would be expected. In turn, the methacrylate used for the model is transparent, while the fiberglass used for a vehicle is opaque and can be painted the same color as the car. Furthermore, the anchoring system is different because the deflector for the model is installed using a groove made on the sides of the car, while a deflector of a real car would have to be anchored to the vehicle or be an integral part of it if it was going to be installed to replace the luggage rack; it could be adapted to the same designs of the three main types of anchorages currently existing: (i) vehicles that have four anchor points, such as a nut, on which the deflector is screwed directly; (ii) when the vehicle has longitudinal bars, the anchoring system on which the transversal bars are fixed is used; (iii) if the vehicle does not have anchor points, it could be installed on four claws that are fastened to the lateral ends of the roof of the vehicle.

The deflector system has a high technical feasibility of implementation, since the anchoring system is similar to that of a luggage rack for storage, and can be placed at the same anchorage points so that the installation is direct and does not require any further modification of the vehicle, neither at the structural level nor at the fastening level. Depending on the type and model of vehicle, it would be necessary to make modifications in the design of the respective hoods, basically due to the different dimensions, varying, in turn, the shape of the curvature of the hood, and the height and inclination of the sides that support the upper sheet, since in each type of vehicle it will be necessary to take into account the volume of incoming air.

However, in the manufacture of new automobiles, the installation of the hood should be considered intrinsically and the design of the vehicle itself should be adapted in such a way that it favors the channeling of the air, in the front part for its collection and in the rear area to optimize the redirection of the flow and the consequent use of the same. One methodology could be to make the upper part of the vehicle with a slightly concave curvature and on the other hand, the hood with a slightly convex curvature to form a shape that tends to be cylindrical, to increase the air intake area.

It is also expected to be socially viable due to the competitive advantages it offers; on the one hand, the economic savings already indicated and also for its environmental benefit, since fortunately social awareness about the environment is becoming more and more rooted, and this deflector system is based on a new methodology for the use of air in the automotive industry, which is a renewable energy source, does not pollute, is inexhaustible and reduces the use of other energy resources, including fossil fuels, the source of greenhouse gas emissions that cause global warming. Therefore, there would be a reduction in CO_2 emissions into the atmosphere, which would reduce the overall carbon footprint. Wind energy is also an indigenous energy source, which contributes to reducing energy imports and any use of wind energy contributes to sustainable development.

4. Conclusions

A channeling system for automobiles has been studied and designed to transform the idea that air is a problem into one of an advantage, by taking advantage of the great force of the airflow incident on the front of the vehicle. The system is based on a cavity-like deflector at the top of the vehicle, which allows air to be captured, channeled, and redirected to the rear vacuum zone, filling it with higher-pressure air.

This makes it possible to (i) reduce the aerodynamic drag caused by the negative pressures of the vacuum zone—by channeling and redirecting the air toward the rear vacuum zone, it fills it by providing higher pressures; (ii) reduce the aerodynamic drag caused by the negative pressures of the vacuum zone and even reaching pressures with positive values, absolute values higher than initial ones; and (iii) solve the problem of vacuum generation at the rear of the vehicles and to favor the propulsion of the vehicle, thanks to the contribution of the airflow channeled through the deflector; it has been proven that this airflow allows the area where a vacuum is conventionally generated with the consequent drag to become an area with positive pressures so that this resistive force can be eliminated and a new driving force has been generated that favors the propulsion of the vehicle.

The effectiveness of the deflector system was first verified by computational modeling, observing that the vacuum zone is filled thanks to the air channeled by the deflector. In addition, experimental tests were carried out, corroborating the computational data through a series of 270 measurements.

The system managed to eliminate a resistance of 4 mm H_2O equivalent to a suction airflow rate of 28.8 km/h, so that, at the same points, the previous resistance was transformed into a forward impulse, the impulse being equivalent to an airflow rate of 15 mm H_2O, i.e., an equivalent air speed of 55 km/h, pushing the car from the rear toward the front, favoring its circulation. Finally, the results found at the technical and performance levels make it favorable to further study this invention to evaluate the potential for its commercial development. To this effect, the authors are intending to initiate a fundraising phase to start the commercial development of this invention after a more thorough study of the real potential of the device.

Author Contributions: Conceptualization, J.F.-G.; methodology, J.F.-G.; formal analysis, J.F.-G., P.F.-A., D.V., and Á.A.-S.; investigation, J.F.-G.; data curation, J.F.-G., P.F.-A., D.V., and Á.A.-S.; writing—original draft preparation, J.F.-G., P.F.-A., D.V., and Á.A.-S.; writing—review and editing, J.F.-G., P.F.-A., D.V., and Á.A.-S.; supervision, P.F.-A., D.V., and Á.A.-S. All authors have read and agreed to the published version of the manuscript.

Funding: This research received no external funding.

Institutional Review Board Statement: Not applicable.

Informed Consent Statement: Not applicable.

Data Availability Statement: All the relevant data of the study are presented in the article.

Conflicts of Interest: The authors declare no conflict of interest.

Appendix A. Comparison of experimental test pressures

Points of the Plane	X (cm)	V (km/h)	Y (mm)	P_α (mm H_2O)			P_β (mm H_2O)			$P_\beta - P_\alpha$ (mm H_2O)		
				Z100	**Z60**	**Z20**	**Z100**	**Z60**	**Z20**	**Z100**	**Z60**	**Z20**
A/B/C	1	35	95	−2	−2	−2	4	4	4	6	6	6
D/E/F			65	−2	−3	−2	0	0	0	2	3	2
G/H/I			35	−2	−2	−2	0	0	0	2	2	2
A/B/C	5		95	−1	−2	−1	4	4	4	5	6	5
D/E/F			65	−2	−3	−2	0	0	0	2	3	2
G/H/I			35	−1	−2	−1	0	0	0	1	2	1
A-B-C	10		95	2	2	2	5	5	5	3	3	3
D-E-F			65	2	3	2	5	5	5	3	2	3
G-H-I			35	2	1	2	4	4	4	2	3	2
A-B-C	20		95	4	4	4	4	5	4	0	1	0
D-E-F			65	4	4	4	4	6	4	0	2	0
G-H-I			35	3	3	3	4	5	4	1	2	1
A-B-C	27		95	4	4	4	5	6	5	1	2	1
D-E-F			65	4	4	4	5	6	5	1	2	1
G-H-I			35	4	4	4	5	6	5	1	2	1
A/B/C	1	41	95	−1	−1	−1	7	7	7	8	8	8
D/E/F			65	−1	−2	−1	0	0	0	1	2	1
G/H/I			35	−1	−1	−1	0	0	0	1	1	1
A/B/C	5		95	−1	−2	−1	5	5	5	6	7	6
D/E/F			65	−2	−3	−2	2	3	2	4	5	4
G/H/I			35	−1	−2	−1	1	2	1	2	4	2
A-B-C	10		95	4	5	4	6	7	6	2	2	2
D-E-F			65	3	3	3	5	6	5	2	3	2
G-H-I			35	4	3	4	4	5	4	0	2	0
A-B-C	20		95	6	7	6	6	7	6	0	0	0
D-E-F			65	5	6	5	5	7	5	0	1	0
G-H-I			35	4	4	4	5	7	5	1	3	1
A-B-C	27		95	6	6	6	6	8	6	0	2	0
D-E-F			65	6	6	6	6	7	6	0	1	0
G-H-I			35	6	6	6	6	7	6	0	1	0
A/B/C	1	50	95	−3	−4	−3	11	11	11	14	15	14
D/E/F			65	−4	−4	−4	0	0	0	4	4	4
G/H/I			35	−4	−4	−4	1	1	1	5	5	5
A/B/C	5		95	−3	−4	−3	10	10	10	13	14	13
D/E/F			65	−3	−5	−3	6	6	6	9	11	9
G/H/I			35	−2	−2	−2	2	2	2	4	4	4

Points of the Plane	X (cm)	V (km/h)	Y (mm)	P_α (mm H_2O)			P_β (mm H_2O)			$P_\beta - P_\alpha$ (mm H_2O)		
				Z100	Z60	Z20	Z100	Z60	Z20	Z100	Z60	Z20
A-B-C	10		95	3	4	3	11	11	11	8	7	8
D-E-F			65	3	4	3	8	11	8	5	7	5
G-H-I			35	3	3	3	6	8	6	3	5	3
A-B-C	20		95	7	9	7	11	12	11	4	3	4
D-E-F			65	6	8	6	9	12	9	3	4	3
G-H-I			35	6	6	6	7	10	7	1	4	1
A-B-C	27		95	8	10	8	10	12	10	2	2	2
D-E-F			65	8	10	8	9	12	10	1	2	2
G-H-I			35	8	8	8	8	11	8	0	3	0

References

1. United Nations Economic Commission for Europe. World Forum for Harmonization of Vehicle Regulations (WP.29). How It Works, How to Join It. New York and Geneva: Economic Commission for Europe, United Nations. Available online: https://unece.org/sites/default/files/2022-07/ECE_TRANS_289_Rev.1_E_corrected.pdf (accessed on 28 November 2022).
2. Ossewaarde, M.; Ossewaarde-Lowtoo, R. The EU's Green Deal: A Third Alternative to Green Growth and Degrowth? *Sustainability* **2020**, *12*, 9825. [CrossRef]
3. Pietrzak, M.B.; Olczyk, M.; Kuc-Czarnecka, M.E. Assessment of the Feasibility of Energy Transformation Processes in European Union Member States. *Energies* **2022**, *15*, 661. [CrossRef]
4. Tian, J.; Yu, L.; Xue, R.; Zhuang, S.; Shan, Y. Global low-carbon energy transition in the post-COVID-19 era. *Appl. Energy* **2022**, *307*, 118205. [CrossRef]
5. Pakulska, T. Green Energy in Central and Eastern European (CEE) Countries: New Challenges on the Path to Sustainable Development. *Energies* **2021**, *14*, 884. [CrossRef]
6. Regulation (EU) 2019/631 of the European Parliament and of the Council of 17 April 2019 Setting CO_2 Emission Performance Standards for New Passenger Cars and for New Light Comercial Vehicles, and Repealing Regulations (ec) no 443/2009 and (eu) no 510/2011. Available online: https://eur-lex.europa.eu/legal-content/es/ALL/?uri=CELEX:32019R0631 (accessed on 25 November 2022).
7. Semeraro, F.F.; Schito, P. Numerical Investigation of the Influence of Tire Deformation and Vehicle Ride Height on the Aerodynamics of Passenger Cars. *Fluids* **2022**, *7*, 47. [CrossRef]
8. Kang, S.O.; Jun, S.O.; Park, H.I.; Song, K.S.; Kee, J.D.; Kim, K.H.; Lee, D.H. Actively translating a rear diffuser device for the aerodynamic drag reduction of a passenger car. *Int. J. Automot. Technol.* **2012**, *13*, 583–592. [CrossRef]
9. Vahdati, M.; Beigmoradi, S.; Batooei, A. Minimising drag coefficient of a hatchback car utilising fractional factorial design algorithm. *Eur. J. Comput. Mech.* **2018**, *27*, 322–341. [CrossRef]
10. Urquhart, M.; Varney, M.; Sebben, S.; Passmore, M. Aerodynamic drag improvements on a square-back vehicle at yaw using a tapered cavity and asymmetric flaps. *Int. J. Heat Fluid Flow* **2020**, *86*, 108737. [CrossRef]
11. Littlewood, R.; Passmore, M. *The Optimization of Roof Trailing Edge Geometry of a Simple Square-Back*; SAE International: Warrendale, PA, USA, 2010. [CrossRef]
12. Yu, X.; Jia, Q.; Yang, Z. Comprehensive Study of the Aerodynamic Influence of Ground and Wheel States on the Notchback DrivAer. *Energies* **2022**, *15*, 1124. [CrossRef]
13. Ha, J.; Jeong, S.; Obayashi, S. Drag reduction of a pickup truck by a rear downward flap. *Int. J. Automot. Technol.* **2011**, *12*, 369–374. [CrossRef]
14. Song, J.; Yoshioka, S.; Kato, T.; Kohama, Y. *Characteristics of Flow Behind a Passenger Vehicle*; SAE International: Warrendale, PA, USA, 2006. [CrossRef]
15. Kurec, K.; Piechna, J. Influence of Side Spoilers on the Aerodynamic Properties of a Sports Car. *Energies* **2019**, *12*, 4697. [CrossRef]
16. Wang, Y.; Sicot, C.; Borée, J.; Grandemange, M. Experimental study of wheel-vehicle aerodynamic interactions. *J. Wind. Eng. Ind. Aerodyn.* **2020**, *198*, 104062. [CrossRef]
17. Afianto, D.; Han, Y.; Yan, P.; Yang, Y.; Elbarghthi, A.F.A.; Wen, C. Optimisation and Efficiency Improvement of Electric Vehicles Using Computational Fluid Dynamics Modelling. *Entropy* **2022**, *24*, 1584. [CrossRef]
18. Lo, K.H.; Kontis, K. Flow around an articulated lorry model. *Exp. Therm. Fluid Sci.* **2017**, *82*, 58–74. [CrossRef]
19. Katz, J.; Garcia, D. *Aerodynamic Effects of Indy Car Components*; SAE International: Warrendale, PA, USA, 2002. [CrossRef]
20. Altaf, A.; Omar, A.A.; Asrar, W. Passive drag reduction of square back road vehicles. *J. Wind. Eng. Ind. Aerodyn.* **2014**, *134*, 30–43. [CrossRef]

21. Piechna, J. A Review of Active Aerodynamic Systems for Road Vehicles. *Energies* **2021**, *14*, 7887. [CrossRef]
22. Piechna, J.R.; Kurec, K.; Broniszewski, J.; Remer, M.; Piechna, A.; Kamieniecki, K.; Bibik, P. Influence of the Car Movable Aerodynamic Elements on Fast Road Car Cornering. *Energies* **2022**, *15*, 689. [CrossRef]
23. Hariram, A.; Koch, T.; Mårdberg, B.; Kyncl, J. A Study in Options to Improve Aerodynamic Profile of Heavy-Duty Vehicles in Europe. *Sustainability* **2019**, *11*, 5519. [CrossRef]
24. Brown, Y.A.; Windsor, S.; Gaylard, A. *The Effect of Base Bleed and Rear Cavities on the Drag of an SUV*; SAE International: Warrendale, PA, USA, 2010. [CrossRef]
25. Sivaraj, G.; Raj, M.G. Optimum way to increase the fuel efficiency of the car using base bleed. *Int. J. Modern Eng. Res.* **2012**, *2*, 1189–1194. Available online: https://api.semanticscholar.org/CorpusID:16934356 (accessed on 1 November 2022).
26. Sivaraj, G.; Parammasivam, K.M.; Suganya, G. Reduction of Aerodynamic Drag Force for Reducing Fuel Consumption in Road Vehicle using Basebleed. *J. Appl. Fluid Mech.* **2018**, *11*, 1489–1495. Available online: https://www.jafmonline.net/article_699_7aa2d948d338b1da8d2a2b1ae9d693f6.pdf (accessed on 1 November 2022). [CrossRef]
27. Al-Saadi, A.; Al-Farhany, K.; Faisal, A.E.; Azeez, M.; Jamshed, W.; Eid, M.R.; Tag, E.S.M.; Ampjad, A. Improvement of the aerodynamic behaviour of the passenger car by using a combine of ditch and base bleed. *Sci. Rep.* **2022**, *12*, 18462. [CrossRef]
28. Urquhart, M.; Varney, M.; Sebben, S.; Passmore, M. Drag reduction mechanisms on a generic square-back vehicle using an optimised yaw-insensitive base cavity. *Exp. Fluids* **2021**, *62*, 241. [CrossRef]
29. Howell, J.; Windsor, S.; Passmore, M. Some Observations on Shape Factors Influencing Aerodynamic Lift on Passenger Cars. *Fluids* **2021**, *6*, 44. [CrossRef]
30. Cerutti, J.J.; Sardu, C.; Cafiero, G.; Iuso, G. Active Flow Control on a Square-Back Road Vehicle. *Fluids* **2020**, *5*, 55. [CrossRef]
31. Littlewood, R.P.; Passmore, M.A. Aerodynamic drag reduction of a simplified squareback vehicle using steady blowing. *Exp. Fluids* **2012**, *53*, 519–529. [CrossRef]
32. Wang, H.; Liu, X.; Chen, T.; Xu, S. Prediction and evaluation of fatigue life via modified energy method considering surface processing. *Int. J. Damage Mech.* **2021**, *31*, 105678952110451. [CrossRef]
33. Yang, X.B.; Liu, X.T.; Tong, J.C.; Wang, Y.S.; Wang, X.L. Research on Load Spectrum Construction of Bench Test Based on Automotive Proving Ground. *J. Test. Eval.* **2018**, *46*, 1099–1110. [CrossRef]
34. Ataei, M.; Tang, C.; Khajepour, A.; Jeon, S. Active camber system for lateral stability improvement of urban vehicles. *Proc. Inst. Mech. Eng. Part D J. Automob. Eng.* **2019**, *233*, 3824–3838. [CrossRef]
35. Muñoz-Caballero, J.; Vergara, D.; Fernández-Arias, P.; Antón-Sancho, Á. Design of a smart barrier to internal flooding. *Inventions* **2022**, *7*, 88. [CrossRef]
36. Desai, S.; Leylek, E.; Lo, C.; Doddegowda, P.; Bychkovsky, A.; George, A.R. *Experimental and CFD Comparative Case Studies of Aerodynamics of Race Car Wings, Underbodies with Wheels, and Motorcycle Flows*; SAE International: Warrendale, PA, USA, 2008. [CrossRef]
37. Schuetz, T.C. *Aerodynamics of Road Vehicles*; SAE International: Warrendale, PA, USA, 2016.
38. Katz, J. *Automotive Aerodynamics*; John Wiley & Sons: Chichester, UK, 2016.
39. Wismer, R.D.; Luth, H.J. Off-road traction prediction for wheeled vehicles. *Trans. ASAE* **1974**, *17*, 8–10. [CrossRef]